Journal of Fluids and Structures (2002) **16**(2), 137–152
doi:10.1006/jfls.2001.0407, available online at http://www.idealibrary.com on IDEAL®

DYNAMICS OF AN IN-LINE TUBE ARRAY SUBJECTED TO STEAM–WATER CROSS-FLOW. PART II: UNSTEADY FLUID FORCES

N. W. Mureithi

Department of Mechanical Engineering, Kobe University, Rokkodai 1-1, Kobe Japan

T. Nakamura, K. Hirota, M. Murata, S. Utsumi

Mitsubishi Heavy Industries Ltd., Takasago R&D Center 2-1-1 Arai-cho, Shinhama Takasago, Hyogo, Japan

T. Kusakabe

Mitsubishi Heavy Industries Ltd., Kobe Shipyard and Machinery Works 1-1 Wadasaki-cho 1-chome, Hyogo-ku, Kobe Japan

AND

H. Takamatsu

The Kansai Electric Power Co. Inc., 3-3-22 Nakanoshima, Kita-ku, Osaka, Japan

(Received 28 October 1999, and in final form 22 May 2001)

In this paper, experimental results of unsteady fluid-force measurements are reported. Important deviations of the measured fluid forces from their single-phase flow counterparts were uncovered. Most importantly, the resulting force coefficients are not simple functions of the reduced flow velocity U/fD, as is the case for single-phase flow. Test results at 0·5 MPa challenge the basic assumption of the existence of a time-invariant linear transfer function between tube displacement and the resulting fluid forces. Time–frequency analysis using Wigner–Ville transforms shows that the phase difference between tube displacement and the fluid force (an indicator of stabilizing or destabilizing fluid effects) undergoes significant variation under what may be considered steady flow conditions. This variation may explain the previously reported phenomenon of intermittent fluidelastic instability in two-phase flows.

1. INTRODUCTION

The existence of fluidelastic instability in two-phase flow has been confirmed experimentally by a number of investigators. In essentially homogeneous two-phase flow, e.g., bubbly flow, it appears that the mechanisms underlying fluidelastic instability and the instability phenomenon are the same as those observed in single-phase flow. The more general case of nonhomogeneous two-phase flow, e.g., slug flow, is less amenable to straightforward interpretation by direct comparison with single-phase flow mechanisms.

For single-phase flow it has been established that fluidelastic instability can be predicted once unsteady fluid-force coefficients have been measured [see for instance, Tanaka & Takahara (1980) and Chen (1983)]. The force coefficients were shown to be functions of reduced flow velocity U/fD. For two-phase flow this single parameter dependency no

0889–9746/02/020137 + 16 $35.00/0

longer holds. The flow pattern and void fraction among other factors, come into play. In fact, for certain flow conditions, the fundamental assumption of the existence of a time-invariant transfer function between tube displacement and fluid forces becomes questionable for two-phase flow. In this paper, we delve into some of these important questions.

We present force coefficient data at high temperature and pressure up to 5·6 MPa, slightly lower than the value of 5·8 MPa at which damping and vibration tests were conducted. Important design challenges, due to the extreme test conditions, are highlighted. The data reduction procedure used to extract the force coefficients is then presented. This analysis we refer to as the averaged analysis. For nonhomogeneous flow conditions, time-dependent effects play an important role in the instability phenomenon. Intermittent instability (Nakamura *et al.* 1995) is caused by nonstationary flow conditions. Time–frequency analysis is performed to gain insight into temporal effects on the force coefficients. The basic mathematical formulation of Wigner–Ville transforms is briefly presented for reference. The bulk of the final results consists of unsteady fluid-force data in two-phase flow for the present array. The application of these data in a stability analysis is presented in the final paper of the series, Hirota *et al.* (2002).

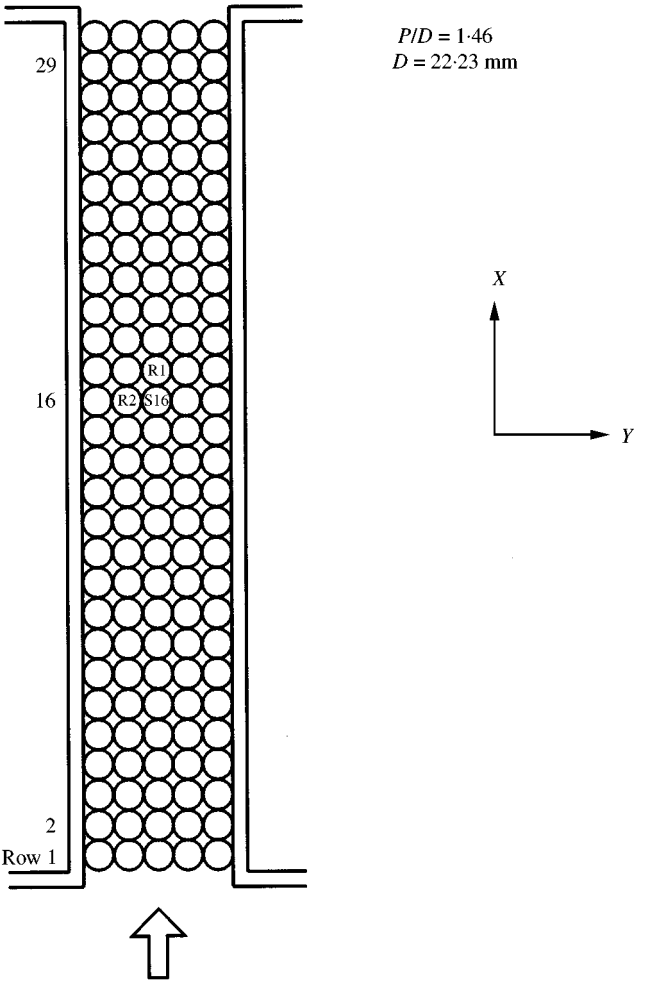

Figure 1. Test array geometry.

2. EXPERIMENTAL APPARATUS AND TEST PROCEDURE

The experimental test-loop and test-array have already been described in Part I of the series (Nakamura *et al.* 2002). For the unsteady fluid-force tests the central part of the array was modified to incorporate strain-gauge instrumented "rigid" tubes for force measurement. The centre tube in row 16 of the array (Figure 1) was the primary test-tube. In addition, two neighbouring tubes identified as R1 (downstream) and R2 (peripheral) were instrumented. Although it would have been desirable to also instrument the tube upstream of S16 as well, the additional cost proved prohibitive.

Figure 2 shows a close-up view of the central measurement region. Tubes R1 and R2 were instrumented in both lift and drag directions. Tube S16 could be rotated to obtain forces in either the lift or the drag direction. A schematic view of the structure of tubes R1 and R2 is shown in Figure 3. The first two natural frequencies are 104·2 and 336·3 Hz. These frequencies are well above the 2–20 Hz measurement range.

Figure 4 shows details of the primary measurement tube. The 161 mm titanium tube, which makes part of the array, moves as a rigid body. It is supported on a larger tube which is ribbed for additional stiffness. The complete structure has a first-mode frequency of 97 Hz. It is supported by a bearing mounted in the test-section wall as shown in Figure 4(a). Excitation was provided by a shaker.

The unbalance force on the bearing at 5·6 MPa test pressure was approximately 1000 kgf. To provide a counter-balancing force, a pressurized cavity exterior to the test-section, at the bearing location, was designed. To determine the balanced condition, a displacement sensor was used to check the axial position of the test-tube against a known zero position

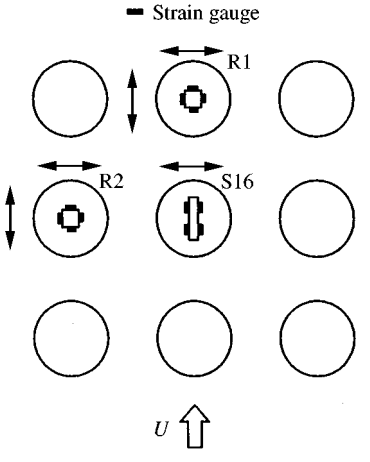

Figure 2. Central measurement area.

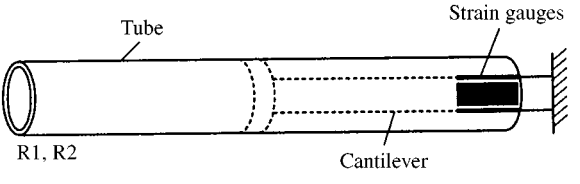

Figure 3. Structure of measurement tubes R1 and R2.

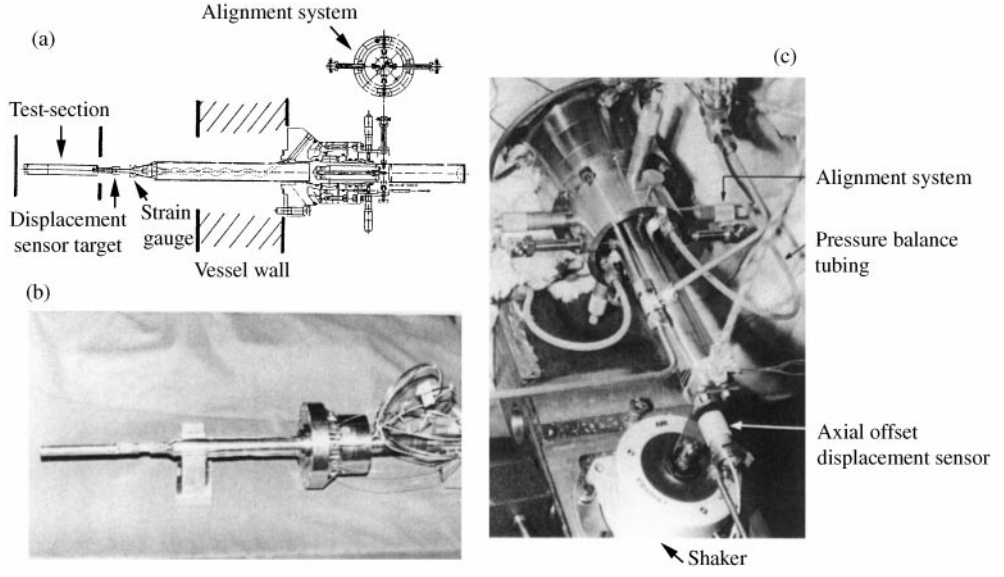

Figure 4. (a, b) Schematic and photo showing primary measurement tube; (c) external view of primary test-tube showing alignment mechanism, pressure balance tubing and shaker.

determined at atmospheric conditions. Nitrogen gas was used to provide the counter-balancing pressure. Tubing for the balancing pressure may be seen in Figure 4(c).

Alignment of the test-tube within the array proved a challenging problem. This was compounded by the limited linear range (0·5 mm) of the eddy-current displacement sensors. An alignment system comprising support wires and micrometers for position checking was designed [Figure 4(a)]. Tube location within the array was confirmed by a pair of displacement sensors, one each for the lift and the drag direction.

For a given pressure setting, the flow velocity was set and allowed to attain a steady state (up to 30 min was required for two-phase flow). The test-tube was then excited at the required amplitude and frequency.

Two measurements were made. First, a time-trace recording of tube S16 displacement and the corresponding fluid forces. Next, a transfer function measurement was performed. Spectral averaging was performed over a period of 4 min for each measurement, to minimize the effect of noise on the measured transfer function. Data obtained included force versus displacement transfer function, auto-spectra and coherence.

3. DATA REDUCTION PROCEDURE

3.1. Time-Averaged Analysis

The measured fluid force per unit length may be expressed as

$$F = \left[\omega^2 \left(m + \frac{\rho D^2}{2} C_{ma} \right) + \mathrm{i}\omega \frac{\rho U D}{2} C_{da} + \frac{\rho U^2}{2} C_s \right] x_0 \, \mathrm{e}^{\mathrm{i}\omega t}, \tag{1}$$

where $x_0 \, \mathrm{e}^{\mathrm{i}\omega t}$ is the displacement of tube S16. Here, C_{ma}, C_{da} and C_s are the fluid added mass, damping and stiffness coefficients, respectively, while m is the tube mass per unit length and D the diameter; U and ρ are the flow velocity and fluid density, respectively.

In homogeneous flow, the fluid force is a stationary quantity. Consequently, the following force/displacement transfer function is defined:

$$H_{Fx} = \frac{F}{x_0 e^{i\omega t}}. \tag{2}$$

The real and imaginary parts of this transfer function take the form

$$\mathscr{R}e[H_{Fx}] = \left[\omega^2\left(m + \frac{\rho D^2}{2} C_{ma}\right) + \frac{\rho U^2}{2} C_s\right], \tag{3a}$$

$$\mathscr{I}m[H_{Fx}] = \left[\omega \frac{\rho UD}{2} C_{da}\right]. \tag{3b}$$

From equation (3) the fluid stiffness force plus added mass component is

$$F_{s,ma} = \mathscr{R}e[H_{Fx}]x_0 - F_{tb}, \tag{4}$$

where the component F_{tb}, related to the tube inertia, has been subtracted; $F_{tb} = m\omega^2 x_0$ for translational tube displacement. Since tube S16 executes a slight rocking motion, F_{tb} was determined by performing tests in air.

The damping force component is given by

$$F_{da} = \mathscr{I}m[H_{Fx}]x_0. \tag{5}$$

Finally, the force coefficient magnitude C_f and phase ϕ_f are given by

$$C_f = \frac{(F_{s,ma}^2 + (\mathscr{I}m[H_{Fx}]x_0)^2)^{1/2}}{\frac{1}{2}\rho U^2 x_0} \tag{6}$$

and

$$\phi_f = \tan^{-1}\left(\frac{\mathscr{I}m[H_{Fx}]x_0}{F_{s,ma}}\right). \tag{7}$$

The data-reduction procedure outlined above is strictly valid only for the transfer function between force and displacement for the moving tube, S16. However, with a slight modification, the analysis is equally valid for transfer functions associated with forces on the fixed tubes, R1 and R2. The inertia terms need to be changed since $F_{tb} = 0$ in this case. Since tubes R1 and R2 are fixed, the mass, m, in equation (1) can be eliminated. C_{ma}, in this case represents a coupling component induced by the motion of tube S16.

In the main results the velocity U is the total superficial gap velocity,

$$U = j_g + j_l. \tag{8}$$

Using equation (5), the damping coefficient becomes

$$c_f = \frac{-\mathscr{I}m[H_{Fx}]}{\omega}, \tag{9}$$

while the corresponding damping factor is

$$\zeta = \frac{-\mathscr{I}m[H_{Fx}]}{2(m + m_a)\omega^2}. \tag{10}$$

The damping ζ is the total fluid damping, including viscous, two-phase and flow-dependent damping as defined in Part I of the paper (Nakamura *et al.* 2002).

For stability analysis, equations (6, 7) give the unsteady fluid forces necessary in the models of Chen (1983) and Tanaka & Takahara (1980).

3.2. Time–Frequency Analysis

In general, forces generated in two-phase intermittent flow are nonstationary, resulting in a time-dependent force–displacement relationship. It is desirable to extend the notion of a classical transfer function to the nonstationary case by simply adding a dimension of time; in other words, a time-dependent "transfer function". In the present study, this translates to the introduction of a time dependence in the fluid-force coefficients in equation (1). Time–frequency signal analysis is a well-developed field with applications in areas such as acoustics and speech analysis, as well as vibration monitoring and diagnosis. The reader is referred to the comprehensive text by Boashash (1992) for reference.

The Wigner–Ville distribution is one of several possible time–frequency signal representations. The cross-Wigner–Ville spectrum between F and x is defined as follows (Claasen & Mecklenbrauker 1980; Boashash & Escudie 1985):

$$W_{Fx}(\omega, t) = \int_{-\infty}^{\infty} \hat{F}\left(t + \frac{\tau}{2}\right) \hat{x}^*\left(t - \frac{\tau}{2}\right) \mathrm{e}^{-\mathrm{i}\omega\tau}\, \mathrm{d}\tau, \tag{11}$$

while the auto-Wigner–Ville transform for x is

$$W_{xx}(\omega, t) = \int_{-\infty}^{\infty} \hat{x}\left(t + \frac{\tau}{2}\right) \hat{x}^*\left(t - \frac{\tau}{2}\right) \mathrm{e}^{-\mathrm{i}\omega\tau}\, \mathrm{d}\tau, \tag{12}$$

where the asterisk indicates complex conjugation. In equations (11) and (12), $\hat{F}$ and $\hat{x}$ are complex analytic representations of the real quantities F and x. As an example

$$\hat{x}(t) = x(t) + \mathrm{i}\tilde{x}(t), \tag{13}$$

where $\tilde{x}(t)$ is the Hilbert transform of $x(t)$, given by

$$\tilde{x}(t) = \frac{1}{\pi} \int_{-\infty}^{\infty} \frac{x(t)}{(t - \tau)}\, \mathrm{d}\tau \bigg|_{P.V.}. \tag{14}$$

P.V. indicates that the Cauchy principal value is to be taken in the integral of equation (14). Instead of the analytic forms, the pure real-time signals F and x may also be used in equations (11, 12). This gives the corresponding Wigner distributions. The Wigner distributions, however, suffer from aliasing (due to negative frequency components), and hence are not desirable. The relation between the Wigner–Ville spectra and the conventional spectra may be demonstrated by the following. Letting $G_F(\omega)$ and $G_x(\omega)$ be the Fourier transforms of F and x, respectively, the integral

$$\int_{-\infty}^{\infty} \mathrm{e}^{-\mathrm{i}\omega t} W_{Fx}\left(\frac{\omega}{2}, t\right) \mathrm{d}t = G_F(\omega) G_x^*(0) \tag{15}$$

shows that the spectrum of F can be recovered up to a constant $G_x^*(0)$. Taking the Fourier transform with respect to frequency instead, $F(t)$ is recovered; thus,

$$\int_{-\infty}^{\infty} \mathrm{e}^{-\mathrm{i}\omega t} W_{Fx}\left(\frac{t}{2}, \omega\right) \mathrm{d}\omega = F(t) x^*(0). \tag{16}$$

W_{Fx} is similar to a cross-spectrum, hence contains phase information; W_{Fx} has the advantage of also containing time as a parameter.

The function W_{Fx} may be expressed as

$$W_{Fx} = \eta(\omega, t) + i\xi(\omega, t), \tag{17}$$

leading to a phase angle definition

$$\phi_f(\omega, t) = \tan^{-1}\left(\frac{\xi(\omega, t)}{\eta(\omega, t)}\right). \tag{18}$$

From equations (11) and (12) the following time-varying equivalent of the transfer function of equation (2) is obtained:

$$H_{Fx}(\omega, t) = \frac{W_{Fx}(\omega, t)}{W_{xx}(\omega, t)}. \tag{19}$$

Considering the real and imaginary parts of $H_{Fx}(\omega, t)$, force coefficients can be extracted by performing analysis identical to that outlined in equations (4–7). The important difference between the resulting force coefficients and the coefficients given by equations (6, 7) is that the force coefficients derived from equation (19) are time-dependent.

In the unsteady fluid-force experiments, the phase angle $\phi_f(\omega_0, t)$ at the tube excitation frequency ω_0 is of interest. The dependence of ϕ_f on time has important implications for stability. A sign change in ϕ_f translates to a sign change in the effective flow-dependent fluid damping, as discussed later.

4. RESULTS

Data presented in what follows are for tests with cross-flow displacement of tube S16. Due to cost limitations the complete set of unsteady fluid-force coefficients could not be measured. As will be apparent, however, the intertube coupling forces are low or have low coherence in two-phase flow, at least for small amplitude displacements.

4.1. Unsteady Fluid Forces at High Pressure

All tests in two-phase flow were conducted for a void fraction of $\beta = 0{\cdot}90$. Figure 5 shows typical time traces at $P = 3{\cdot}0$ MPa for the tube (S16), cross-flow displacement and corresponding fluid forces on the three measurement test-tubes; the flow velocities are $j_g = 0{\cdot}9$ m/s, $j_l = 0{\cdot}10$ m/s and excitation frequency 15 Hz. In all tests at $P = 5{\cdot}6$ MPa, tube S16 was oscillated in cross-flow with a peak amplitude $x_0 = 0{\cdot}145$ mm. For tube S16, a large displacement-dependent force is generated. Note, however, that this includes a component due to tube inertia. On the other hand, the force on the neighbouring tubes is seen to be primarily due to turbulent buffeting. The amplitude x_0 was limited by the extreme load on the tube support O-ring seals due to the pressure discontinuity at the vessel wall.

Figure 6 shows an example of the lift-direction fluid force coefficients as a function of U/fD for tube S16. The data corresponds to $U = 1{\cdot}0$ m/s and $2{\cdot}3$ m/s at the highest pressure $P = 5{\cdot}6$ MPa. The excitation frequencies are 20, 15, 10, 5 and 2 Hz. It is clear that unlike the case of single-phase flow (Tanaka & Takahara 1980; Chen 1983; Mureithi *et al.* 1996), the force coefficients are not simple single-valued functions of U/fD. At constant U/fD, the force coefficients show variation depending on the combination of U and f. This indicates that the homogeneous velocity may not be the true independent parameter. Alternatively, it is suspected that a single, simple independent parameter may not exist. The above phenomenon is most prominent at 0·5 MPa pressure, as seen in Figure 7 for tests at the same velocities and frequencies as the data of Figure 6 with S16 excitation amplitude,

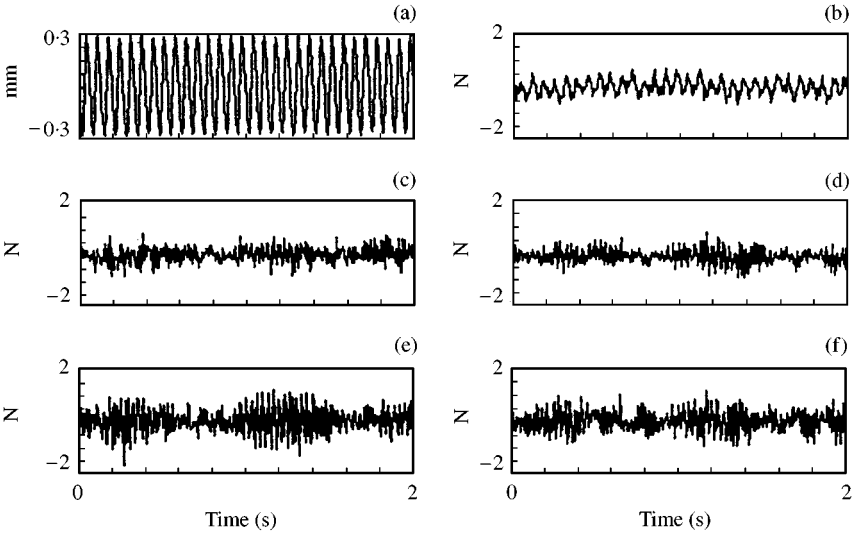

Figure 5. Typical time-trace data for 15 Hz excitation ($P = 3{\cdot}0$ MPa, $j_g = 0{\cdot}9$ m/s, $j_l = 0{\cdot}10$ m/s): (a, b) tube S16 cross-flow displacement; (c, d) tube R1 drag and lift forces; (e, f) tube R2 drag and lift forces.

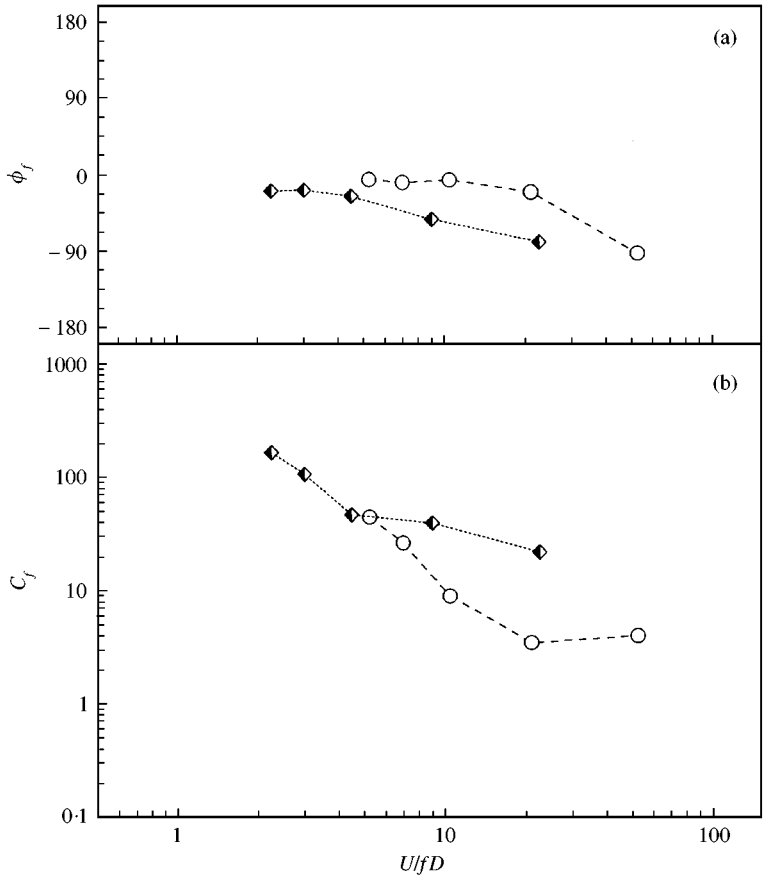

Figure 6. Tube S16 lift force coefficient dependence on U/fD at $P = 5{\cdot}6$ MPa for: ○, $U = 1{\cdot}0$ m/s; ◐, $U = 2{\cdot}3$ m/s. (a) Phase, (b) magnitude.

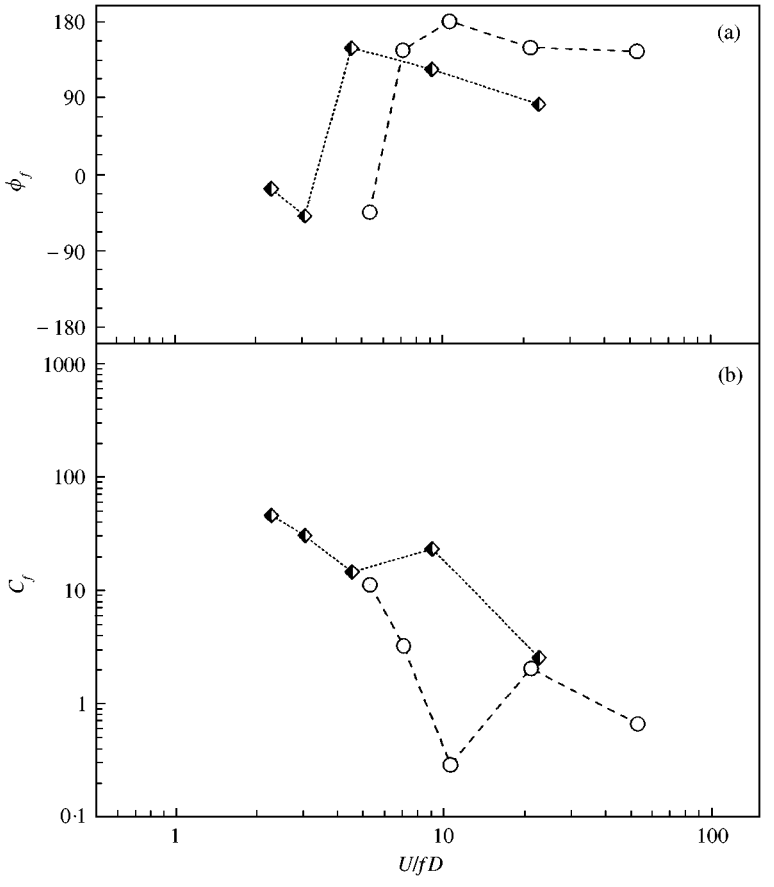

Figure 7. Tube S16 lift force coefficient dependence on U/fD at $P = 0{\cdot}5$ MPa for: ○, $U = 1{\cdot}0$ m/s; ◐, $U = 2{\cdot}3$ m/s. (a) Phase, (b) magnitude.

$x_0 = 0{\cdot}65$ mm. The phase shows an apparent shift with U/fD as U increases. Note, however, that the trend with U/fD (at fixed U) is maintained. C_f on the other hand is not shifted as U increases. However, in the range $4 < U/fD < 25$, C_f is multivalued. This becomes more apparent later in Figure 10 for this pressure.

For the highest pressure, 5·6 MPa, the force coefficient magnitude and phase are shown in Figure 8. For each tube, the coherence between the fluid force and tube S16 displacement is also shown. This is the complete set of force-coefficient data taken for the three tubes: S16, R1 and R2. Data taken at a constant flow velocity U (for varying frequency) are indicated by the same symbol. Tube S16 (cross-flow) amplitude is $x_0 = 0{\cdot}145$ mm.

For tube S16, the phase angle ϕ_f, Figure 8(a), is negative at low U/fD. Recalling that negative ϕ_f corresponds to positive damping [equations (7, 10)], for low U/fD the presence of two-phase damping, ζ_{tp}, is evident. This is in contrast to the single-phase flow case where only a small amount of viscous damping exists at low U/fD, hence $\phi_f \approx 0$ but slightly negative. The limiting value of ϕ_f, as U/fD approaches zero, gives an estimate of the flow-independent two-phase damping, ζ_{tp}, defined in Part I of the series (Nakamura *et al.* 2002).

Above $U/fD \approx 5$, the variation of ϕ_f (with U/fD) is significantly different from the single-phase flow case. In the latter, ϕ_f becomes large and positive. This transition does not

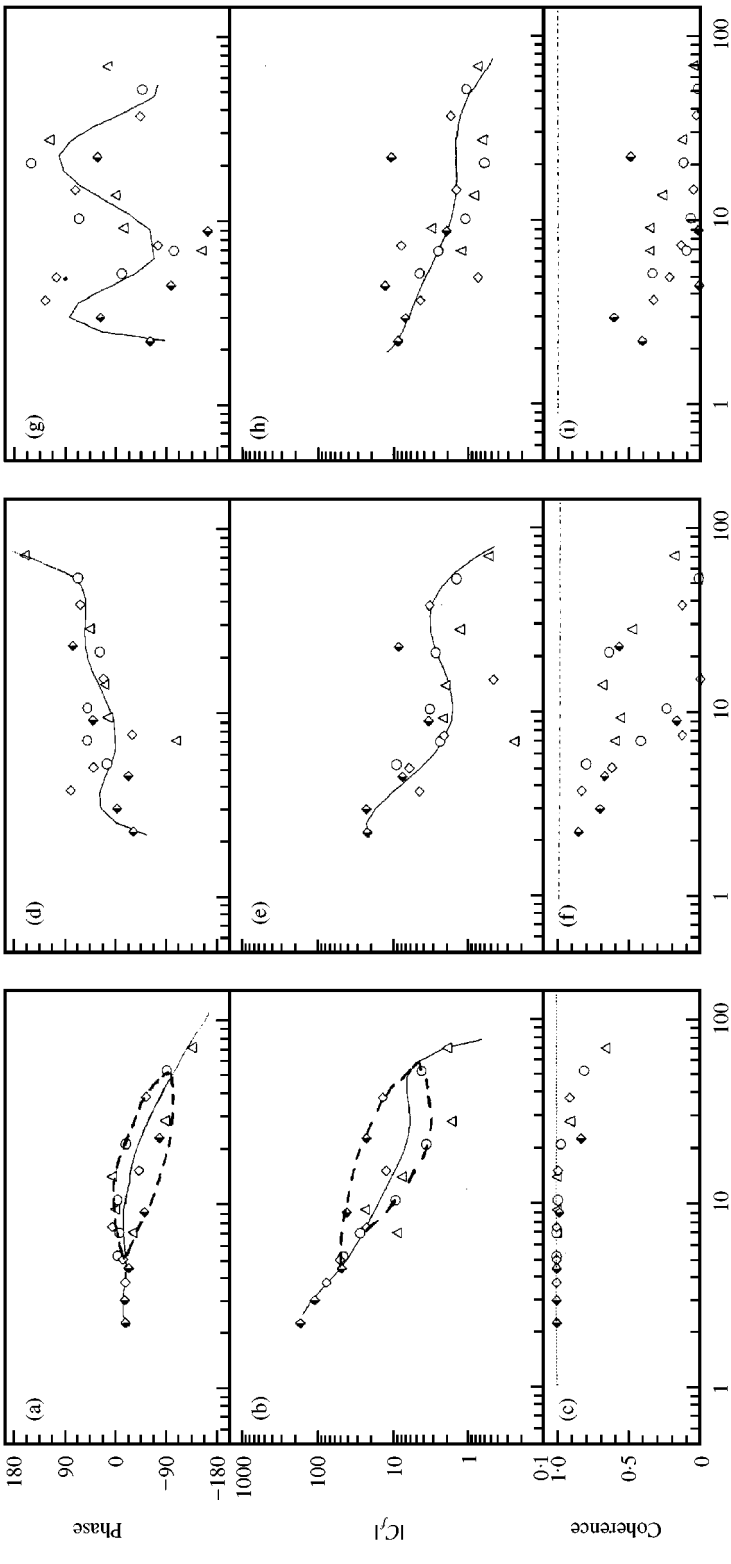

Figure 8. Force coefficient phase, magnitude and coherence for: (a–c) tube S16, lift; (d–f) tube R1, lift; (g–i) tube R2, lift; $P = 5{\cdot}6$ MPa. Fluid velocities (j_g, j_l) are: ◆, (0·10, 0·9); ◇, (0·17, 1·5); ○, (0·23, 2·1); △, (0·31, 2·8).

occur for the 5·6 MPa tests for the range of U/fD tested. Instead, ϕ_f becomes increasingly negative after a brief upward trend near $U/fD = 10$. In Figure 8(a, b) the result of a polynomial fit on the data is shown as a solid line. In the range $5 \leqslant U/fD \leqslant 50$, it appears that both C_f and ϕ_f are better represented by double-valued functions. In each case, two branches are indicated by broken lines. The ϕ_f and C_f data for $U = 1{\cdot}00$ m/s ($j_g = 0{\cdot}9$ m/s, $j_l = 0{\cdot}10$ m/s) fall on the lower and upper branches, respectively, in the corresponding graphs. Data for $U = 2{\cdot}33$ m/s ($j_g = 2{\cdot}1$ m/s, $j_l = 0{\cdot}23$ m/s), on the other hand, fall on the opposite branches [Figure 8(a, b)]. Although results are less clear for other test velocities, correspondence with the indicated branches is still remarkable. The multivalued nature of the force coefficients may not be entirely unexpected. Single-phase data shows that C_f and ϕ_f undergo a sharp discontinuity near $U/fD = 10$ for tube S16. This is associated with a change in the local flow structure. The appearance of two branches in Figure 8(a, b) might indicate that two-phase flow behaves differently from single-phase flow in this transition region; essentially two possible stable flow configurations exist.

For the neighbouring tubes R1 and R2, no clear branching in C_f and ϕ_f data is evident [Figure 8(d–i)], although multiple values of C_f and ϕ_f occur at a given U/fD. In the case of ϕ_f [Figure 8(d, g)], the polynomial fit is a reasonable indicator of the data trend. C_f, on the other hand, may still be better approximated by a multiple-valued function as is most distinctly evident in Figure 8(e).

The coherence between the measured fluid forces and tube (S16) displacement is also presented in Figure 8. As expected, coherence is high for tube S16, Figure 8(c). Significantly lower values are obtained for the coupling forces on tubes R1 and R2. Low coherence is an indicator of the presence of noise (turbulence excitation in this case) and/or nonlinear effects. While low coherence due to noise has negative implications on measurement accuracy, long-time averaging (4 min in the present tests) can counter the effect of reduced coherence. Physically, low coherence implies that instability involving coupled tube motion is less likely to be initiated than in the case where coherence is unity.

At 3·0 MPa pressure, a higher tube (S16) amplitude of 0·30 mm peak could be attained in the tests. Figure 9 shows the resulting force coefficients. Data for the central tube (S16) are once again multivalued in the intermediate range of U/fD. The transition in ϕ_f is similar to that observed in single-phase flow, albeit occurring at much higher U/fD (here near $U/fD = 30$ versus $U/fD = 10$ in single-phase flow). C_f is slightly lower at 3·0 MPa than at 5·6 MPa for tube S16. For the neighbouring tubes, C_f values are close for both pressures, while the scatter in ϕ_f data (for R1 and R2) makes comparison difficult. The overall trend of ϕ_f for tube R2 (-180° at low U/fD and increasing monotonically with U/fD) is similar to that obtained in single-phase flow [see Tanaka & Takahara (1980)].

Next, the results of tests at $P = 0{\cdot}5$ MPa are presented. In this case, the S16 test tube was oscillated with a peak amplitude of 0·65 mm. C_f and ϕ_f show no clear relationship with U/fD, as seen in Figure 10.

The flow structure approaches slug-type flow at 0·5 MPa pressure [see Appendix A in Nakamura *et al.* (2002)]. The fluid forces are therefore strongly time-dependent. In this case, the existence of some time-averaged transfer function is questionable. One can easily imagine that the instantaneous fluid force and phase change as ambient flow changes from gas to liquid. The resulting fluid forces are therefore nonstationary quantities. In this case, the idea of a (constant) linear transfer function is invalid. It is therefore necessary to incorporate temporal effects in the force–displacement relation. The effect of fluid force nonstationarity is considered in the section on time–frequency analysis which follows.

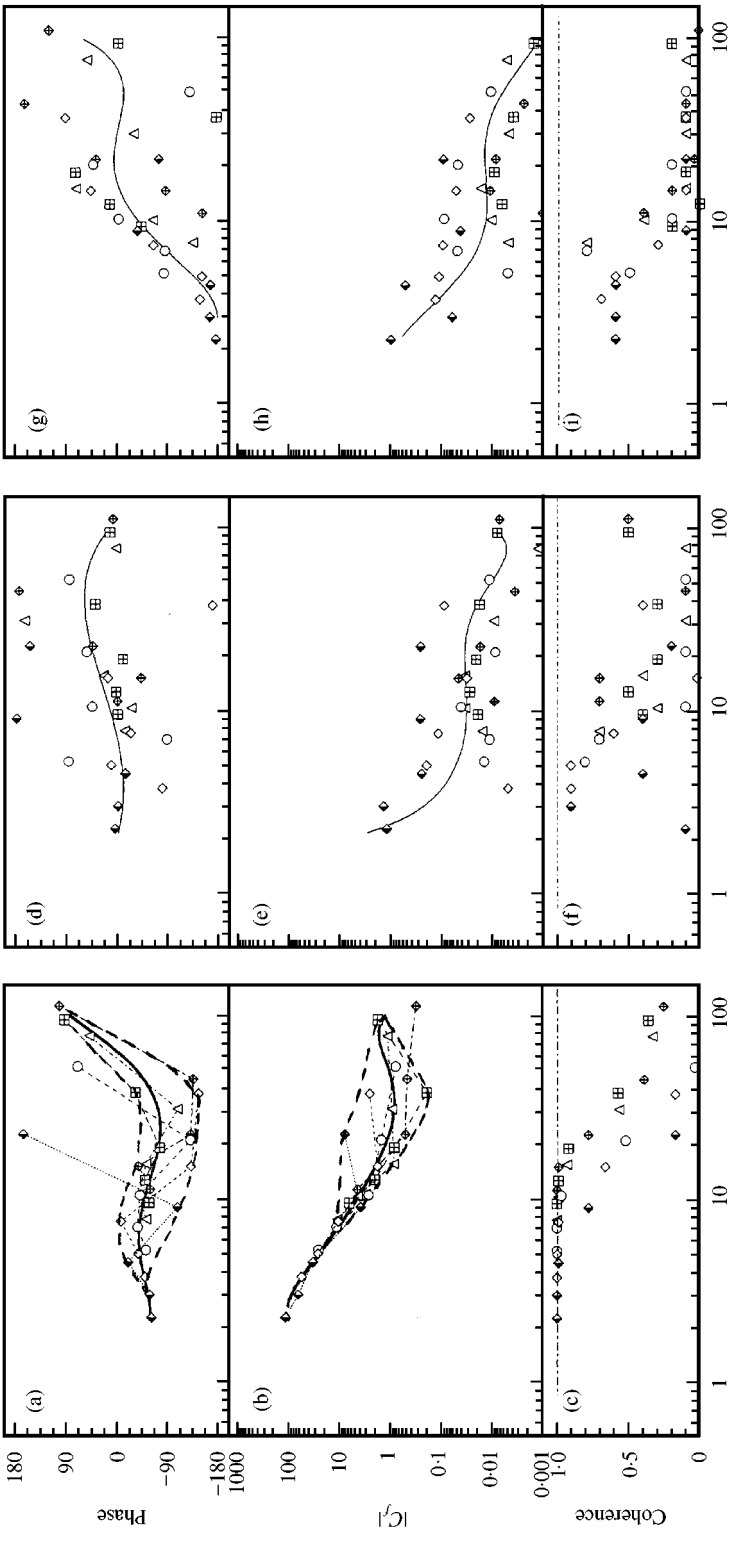

Figure 9. Force coefficient phase, magnitude and coherence for: (a–c) tube S16, lift; (d–f) tube R1, lift; (g–i) tube R2, lift; $P = 3{\cdot}0$ MPa, $x_0 = 0{\cdot}300$ mm. Fluid velocities (j_g, j_l) are: ◆, (0·10, 0·9); ◇, (0·17, 1·5); ○, (0·23, 2·1); △, (0·34, 3·1); ⊞, (0·42, 3·8) and ⊕, (0·50, 4·5).

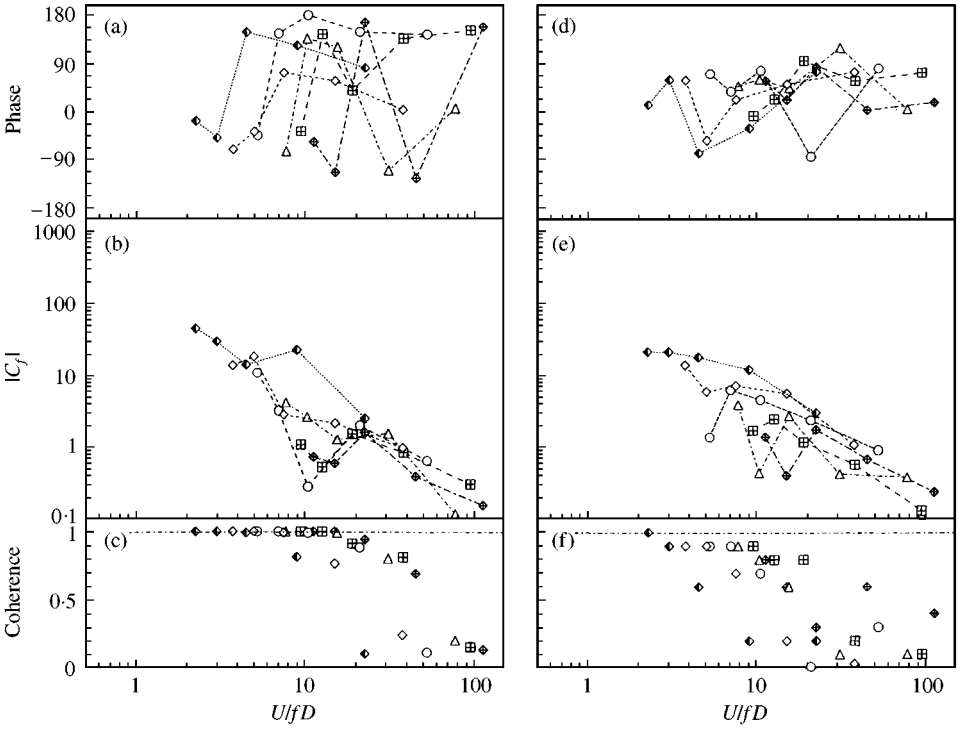

Figure 10. Force coefficient phase, magnitude and coherence for: (a–c) tube S16, lift; (d–f) tube R1, lift; $P = 0{\cdot}5$ MPa, $x_0 = 0{\cdot}650$ mm. Fluid velocities (j_g, j_l) are: ◆, (0·10, 0·9); ◇, (0·17, 1·5); ○, (0·23, 2·1); △, (0·34, 3·1); ⊞, (0·42, 3·8) and ⊕ (0·50, 4·5).

4.2. Time–Frequency Analysis

It was noted above that for nonhomogeneous flows, the assumption of existence of an average transfer function is invalidated by nonstationarity of the fluid forces. A rigorous check was conducted by performing a Wigner–Ville transform analysis on data at 5·6 (homogeneous flow) and 0·5 MPa (nonhomogeneous flow). From auto- and cross-Wigner–Ville transforms, a continuous representation of the transfer function in time can be derived. The mathematical representation is given by equation (19).

Figure 11(a, b) shows tube S16 fluid-force time traces for tests at $j_l = 0{\cdot}10$ m/s, $j_g = 0{\cdot}9$ m/s, and tube excitation frequency $f = 20$ Hz for $P = 5{\cdot}6$ MPa and 10 Hz for 0·5 MPa, respectively. The frequency spectrum for $P = 0{\cdot}5$ MPa was found to be strongly time-dependent indicating nonstationarity of the fluid force. Figure 11(c, d) shows the force–displacement phase difference $\phi_f(\omega, t)$ derived from $W_{Fx}(\omega, t)$, equation (18), for $P = 5{\cdot}6$ and 0·5 MPa. While the phase is constant (as expected) for 5·6 MPa, large variations occur for 0·5 MPa. Physically, this means that the instantaneous damping force varies between positive and negative values over time for $P = 0{\cdot}5$ MPa. Since the phase may stay, say, positive over several oscillation cycles, instability can occur. This instability is, however, reversed several cycles later. This may explain the phenomenon of intermittent instability common in two-phase flow [see, e.g., Nakamura *et al.* (1995)].

From the foregoing it is clear that the time-averaged force coefficients presented in Figure 10 (for $P = 0{\cdot}5$ MPa) may not yield the correct instability boundary. A stability analysis taking temporal effects into account is needed. Such an analysis has been proposed by Nakamura *et al.* (1995).

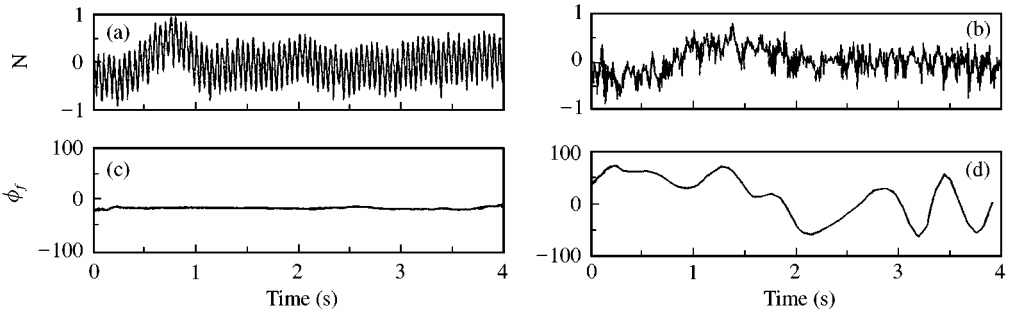

Figure 11. (a, b) Tube S16 lift direction fluid-force time traces for $U = 1{\cdot}00$ m/s; (c, d) variation with time of force/displacement phase difference from Wigner–Ville transform. Test conditions are: (a, c) $P = 5{\cdot}6$ MPa, $f = 20$ Hz and (b, d) $P = 0{\cdot}5$ MPa, $f = 10$ Hz.

TABLE 1

Two-phase damping for tube S16, in the cross-flow direction, determined by measurement compared with values calculated from unsteady fluid force; ($\beta = 0{\cdot}90$)

		ζ_{tp} (%)	
P (MPa)	U/fD	Direct damping test	Fluid-force test
3·0	2·2	1·7	1·9
5·8, 5·6	2·3	1·1	0·9

4.3. ESTIMATION OF TWO-PHASE FLOW DAMPING

We now briefly return to the question of two-phase flow damping, discussed at length in Part I of this study (Nakamura *et al.* 2002).

Two-phase damping (ζ_{tp}) was defined as the damping value in the limit of zero flow velocity (excluding viscous damping, ζ_v). The fluid damping force at low U/fD consists of components ζ_{tp} and ζ_v. By theoretically estimating ζ_v, it becomes possible to determine two-phase damping, ζ_{tp}, from the measured unsteady fluid forces. Also, ζ_v may be theoretically estimated by (Chen *et al.* 1976; Rogers *et al.* 1984)

$$\zeta_v = \frac{\pi}{\sqrt{8}} \left(\frac{\rho D^2}{m + m_a} \right) \left(\frac{2v}{\pi f D^2} \right)^{1/2} \left[\frac{1 + (D/D_e)^3}{(1 - (D/D_e)^2)^2} \right], \tag{20}$$

where ρ and v are homogeneous density and viscosity, respectively. From equations (9, 10) then we have

$$\zeta_{tp} = \frac{c_f}{2(m_a + m)\omega} - \zeta_v, \tag{21}$$

with the viscous damping as given by equation (20).

Table 1 shows the comparison between ζ_{tp} as measured directly (Nakamura *et al.* 2002) and as given by equation (21), for tube S16 and $\beta = 0{\cdot}90$. Agreement is quite reasonable. Figure 12 shows the variation of ζ with U/fD for $P = 5{\cdot}6$ (and 5·8) MPa. The value shown in Table 1 (for 5·6 MPa) corresponds to the data at the lowest U/fD in Figure 12. It is clear

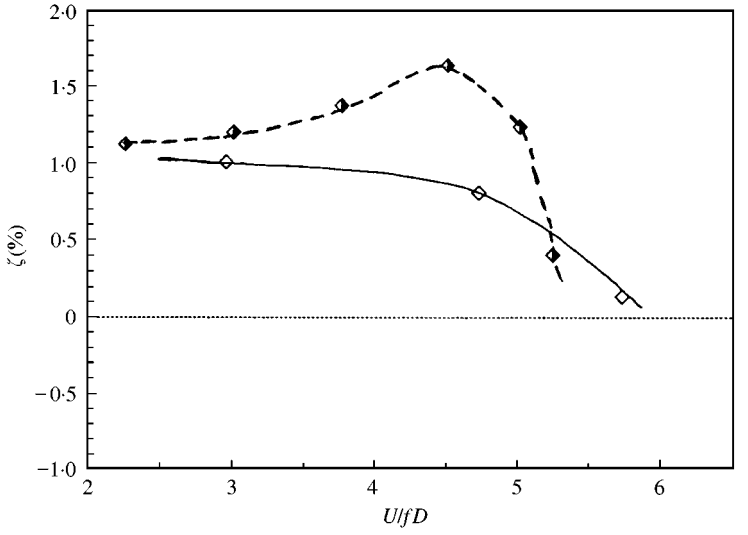

Figure 12. Comparison of fluid damping from (a) ◆, unsteady fluid forces tests, $P = 5{\cdot}6$ MPa, (b) ◇, direct damping measurement, $P = 5{\cdot}8$ MPa. Data are for tube S16 (cross-flow direction), and void fraction $\beta = 0{\cdot}90$.

that ζ_{tp} is hardly small and, as a result, modifies the measured fluid forces considerably. Since ζ_{tp} is considered to be independent of U/fD, it is reasonable to subtract the corresponding damping force, $2(m + m_a)\zeta_{tp}\omega x_0$, together with a similar component due to viscous damping, ζ_v, from the total damping force [F_{da} in equation (5)]. The result is new values $\bar{C}_f$ and $\bar{\phi}_f$ [see equations (6, 7)] which are independent of ζ_{tp} and ζ_v; $\bar{\phi}_f$ is identical to ϕ_f except for a shift: $\phi_f = \bar{\phi}_f - \phi_0$, where ϕ_0 is the phase difference induced by $\zeta_{tp} + \zeta_v$.

5. SUMMARY AND CONCLUSIONS

Unsteady fluid forces at high temperature and pressure (prototypical conditions) in steam–water flow have been measured. Significant differences from the case of single-phase flow were found. At high pressure ($P \geq 3{\cdot}0$ MPa), the cross-flow direction fluid-force coefficients associated with a tube's own motion is double valued in the intermediate U/fD range, $5 \lesssim U/fD \lesssim 50$. Intertube coupling forces are also multivalued at a given U/fD, although clear branching is not self-evident. Two-phase damping, ζ_{tp}, adds a significant component to the measured damping force. This component (together with the viscous damping force) should be subtracted from the total measured force in order to obtain the true flow-dependent unsteady fluid force.

In nonhomogeneous flow (0·5 MPa), the assumption of the existence of a transfer function between fluid force and tube displacement was shown to break down. A time–frequency analysis confirmed that the instantaneous transfer function is strongly time-dependent. This could lead to intermittent instabilities.

Unlike the case of single-phase flow, the unsteady fluid forces in two-phase flow are complex functions of reduced velocity, void fraction and other parameters. This necessarily complicates the application of these forces in a stability analysis. The low coherence associated with intertube coupling forces is another significant result. This essentially reduces the probability of *initiation* of a coupled-mode instability.

ACKNOWLEDGEMENTS

K. Yoshikawa conducted the calibration, extensive pretesting and assembly of the experimental apparatus. Tests were principally conducted by K. Mitsumori. The authors sincerely acknowledge their invaluable contribution.

This work was jointly financed by Mitsubishi Heavy Industries and the five electric power companies operating PWRs in Japan (Kansai Electric, Shikoku Electric, Kyushu Electric, Hokkaido Electric and Japan Atomic Power Company).

REFERENCES

BOASHASH, B. (ed.) 1992 *Time–Frequency Signal Analysis — Methods & Applications.* Melbourne: Longman.

BOASHASH, B. & ESCUDIE, B. 1985 Wigner–Ville analysis of asymptotic signals and applications. *Signal Processing* **8,** 315–327.

CHEN, S. S. 1983 Instability mechanisms and stability criteria of a group of circular cylinders subjected to cross-flow. Parts I & II. *Journal of Vibration, Acoustics, Stress and Reliability in Design* **105,** 51–58 and 253–260.

CHEN, S. S., WAMBSGANSS, M. W. & JENDREZEJCZYK, J. A. 1976 Added mass and damping of a vibrating rod in confined viscous fluids. *Journal of Applied Mechanics* **43,** 325–329.

CLAASEN, T. A. C. M. & MECKLENBRAUKER, W. F. G. 1980 The Wigner distribution — a tool for time–frequency signal analysis. *Philips Journal of Research* **35,** 217–250.

HIROTA, K., NAKAMURA, T., MUREITHI, N. W., KASAHARA, J., KUSAKABE, T. & TAKAMATSU, H. 2002 Dynamics of an in-line tube array subjected to steam–water cross-flow. Part III: fluideslastic instability tests and comparison with theory. *Journal of Fluids and Structures* **16,** 153–173.

MUREITHI, N. W., NAKAMURA, T., HIROTA, K., MURATA, M., UTSUMI, S., KUSAKABE, T. & TAKAMATSU, H. 1996 Dynamics of an inline tube array in steam–water flow. Part II: unsteady fluid forces. In *Flow-Induced Vibration 1996* (ed. M. J. Pettigrew), PVP Vol. 328, pp. 111–121. New York: ASME.

NAKAMURA, T., FUJITA, K., KAWANISHI, K., YAMAGUCHI, N. & TSUGE, A. 1995 Study on the vibrational characteristics of a tube array caused by two-phase flow. Part II: Fluidelastic vibration. *Journal of Fluids and Structures* **9,** 519–538.

NAKAMURA, T., MUREITHI, N. W., HIROTA, K., MURATA, M., UTSUMI, S., KUSAKABE, T. & TAKAMATSU, H. 2002 Dynamics of an in-line tube array subjected to steam–water cross-flow. Part I: two-phase damping and added mass. *Journal of Fluids and Structures* **16,** 123–136.

ROGERS, R. J., TAYLOR, C. & PETTIGREW, M. J. 1984 Fluid effects on multi-span heat exchanger tube vibration. In *Proceedings of the ASME-PVP Conference*, San Antonio, TX, U.S.A.

TANAKA, H. & TAKAHARA, S. 1980 Unsteady fluid dynamic force on tube bundle and its dynamic effect on vibration. In *Flow-Induced Vibration of Power Plant Components*, (ed. M. K. Au-Yang), PVP- Vol. 41, pp. 77–92. New York: ASME.